THE JOURNAL OF PHYSICAL CHEMISTRY C

Article

Cite This: J. Phys. Chem. C 2019, 123, 17855−17863

pubs.acs.org/JPCC

Sticking Probability of High-Energy Methane on Crystalline, Amorphous, and Porous Amorphous Ice Films

Published as part of The Journal of Physical Chemistry virtual special issue "Hai-Lung Dai Festschrift".

Rebecca S. Thompson, Michelle R. Brann, and S. J. Sibener*

The James Franck Institute and Department of Chemistry, The University of Chicago, 929 East 57th Street, Chicago, Illinois 60637, United States

ABSTRACT: We present research detailing the sticking probability of CH_4 on various D_2O ices of terrestrial and astrophysical interest using a combination of time-resolved, *in situ* reflection absorption infrared spectroscopy (RAIRS) and King and Wells mass spectrometry techniques. As the incident translational energy of CH_4 increases (up to 1.8 eV), the sticking probability decreases for all ice films studied, which include high-density, non-porous amorphous (np-ASW), and crystalline (CI) films as well as porous amorphous (p-ASW) films with various pore morphologies. Importantly, sticking probabilities for all p-ASW films diverge and remain higher than either np-ASW or CI films at the highest translational energies studied. This trend is consistent across all porous morphologies studied and does not depend on pore size or orientation relative to the substrate. It is proposed that in addition to offering slightly higher binding energies the porous network in the D_2O film is very efficient at dissipating the energy of the incident CH_4 molecule. These results offer a clear picture of the initial adsorption of small molecules on various icy interfaces; a quantitative understanding of these mechanisms is essential for the accurate modeling of many astrophysical processes occurring on the surface of icy dust particles.

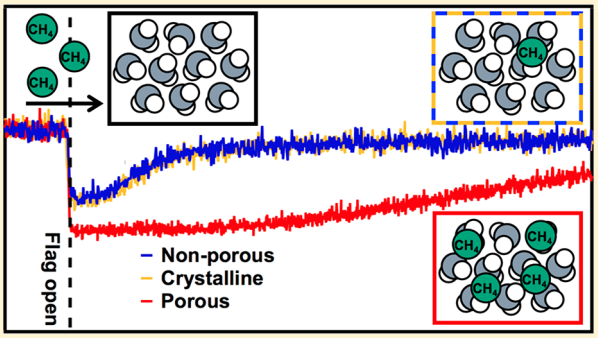

INTRODUCTION

Examining molecular and atomic adsorption onto frozen water ices is necessary to create accurate models of the chemical and physical processes occurring in atmospheric and terrestrial environments.[1,2] Furthermore, understanding the interactions between gas molecules and different molecular ices can help to classify the composition and the history of complex multicomponent ices.[3] Adsorption on icy surfaces, in astrophysical environments for instance, is a critical first step in a variety of recombination and addition reactions, some resulting in the formation of small organic molecules.[4,5]

Ice can exist in a variety of crystalline and amorphous forms. Crystalline (CI) water ice with its hexagonal lattice is the most common form of snow and ice on Earth[6] and can also be found in warmer astrophysical environments.[7] Amorphous solid water (ASW), on the other hand, is the most abundant form of water in astrophysical environments[8] and is present in comets, planetary rings, and interstellar clouds.[9] ASW can be classified into two types: high-density non-porous (np-ASW) and low-density porous (p-ASW) based on its pore structure.[10] In general, ASW morphology plays a significant role in the adsorption of volatile gas species within astrophysical ices.[11−13] Although not yet found in such environments, p-ASW can exist as the result of heterogeneous molecular synthesis occurring on dust grains in the interstellar medium (ISM).[14] Exposure to ultraviolet light, X-rays, cosmic radiation, or thermal processing can also induce morphological changes in astrophysical ices.[2,13−15] Over time and as a result of these processes, ASW ices can become CI and vice versa. Because of this, there is an interest in understanding the precise role of surface morphology in gaseous adsorption.[16]

This work uses high-energy projectiles to examine adsorption mechanisms on various astrophysical ices. A particular focus is on porous amorphous water ices and how the pore structure influences the energy accommodation and uptake of incident molecules. In general, a molecule impacting a surface adsorbs if it loses enough of its kinetic energy to the lattice upon impact.[17] Accurate measurements of sticking probabilities are essential because a higher sticking probability can lead to greater observed reactivity as has been shown for a variety of molecules on amorphous ices.[18]

We present the first study examining the sticking probability of CH_4 as a function of translational beam energy on p-ASW of varying porosities, np-ASW, and CI D_2O ice films under ultrahigh vacuum (UHV) using the King and Wells method and molecular beam techniques.[19] Molecular beams enable tunable control of incident energy and thus precise knowledge of the sticking process.[20] CH_4 was chosen primarily due to its known presence in many astrophysical environments, including its potential incorporation in icy clathrates found in outer solar

Received: April 25, 2019
Revised: June 26, 2019
Published: July 15, 2019

DOI: 10.1021/acs.jpcc.9b03900
J. Phys. Chem. C 2019, 123, 17855−17863

system bodies such as Titan.[14,21,22] Within those environments, reactions involving CH_4 can be a significant contributor to the formation of complex organic molecules.[23] Additionally, CH_4 allows us to exclusively probe adsorption phenomena because its light mass and lower momenta may preclude direct embedding underneath the surface.[24−26] We demonstrate that for the highest energy beam (1.8 eV) the sticking probability is higher for p-ASW than np-ASW and CI ices. For the p-ASW ices, we also determine that there is no difference in sticking probability as a result of increased porosity.

Our results build upon previous work in our group focused on the sticking probability of D_2O and H_2O on CI for incident translation energies ranging from 0.3 to 0.7 eV.[27] The sticking probability was near unity for those measurements and did not change as a function of water ice morphology or surface temperatures ranging from 140 to 155 K. By using CH_4 and expanding the water ice morphology to include amorphous water ices with and without pores as well as higher incident translational energies, our measurements provide a more complete understanding of the dynamics of sticking between projectiles and water ices. Such work is critical to creating accurate models of these processes occurring in atmospheric and terrestrial environments between water ices and CH_4. By examining the initial part of the uptake process, these results provide insight into the adsorption−desorption equilibrium for ices in the troposphere.[28] Beyond these astrophysical and environmental applications, the adsorption of molecules into solid materials is an important first step in many dynamic processes at interfaces in fields such as photocatalysis, radiation chemistry, waste processing, and advanced materials synthesis.[11] Many commercial catalysts are porous within these fields; these pore structures enable efficient sticking and transport of molecules.[29]

EXPERIMENTAL SECTION

All experiments were conducted in a molecular beam scattering instrument previously discussed in full detail.[27] Generally, this instrument consists of a UHV chamber with base pressures of 10^{-10} Torr connected to a triply differentially pumped molecular beamline. Inside the chamber, a state-of-the-art helium-cooled sample manipulator (Advanced Research Systems) enables precise and accurate temperature control of the Au(111) sample substrate between 20 and 800 K. The crystal is exposed to the beam and monitored in real time with optics for *in situ* reflection absorption infrared spectroscopy (RAIRS). Gas scattering and incident flux are also monitored with a residual gas analyzer (RGA).

All RAIR spectra are analyzed with Gaussian peaks atop either linear or cubic baselines, depending on the region. Spectra were acquired with a Nicolet 6700 infrared spectrophotometer (Thermo Fisher) using incident *p*-polarized IR radiation at an angle of 75° to the Au(111) crystal and a liquid-nitrogen-cooled mercury cadmium telluride (MCT/A) detector. Each RAIR spectrum is an average of 70−200 scans taken using 4 cm^{-1} resolution with a clean Au(111) sample for the background. For ice preparation, D_2O was chosen (rather than H_2O) due to its preferable O−D stretch frequency that avoids overlap with the ν_3 methane mode.[30−32]

D_2O films were produced via a directed doser at a 30° angle and approximately 4 cm from the Au(111) crystal. D_2O was typically leaked in at a pressure of 2.0×10^{-9} Torr, leading to an average growth rate of 0.5 ML/min.[33] The ice films used in this study were between 150 and 300 layers thick. Film thickness was determined by backfilling the UHV chamber to a pressure of 1.0×10^{-7} Torr D_2O, which corresponds to a growth rate of 0.1 ML/s. RAIR spectra were collected at regular time intervals during exposure, which allowed for direct quantification of film thickness from integrated intensity of the large O−D stretch between 3600 and 2800 cm^{-1}.[34,35] Figure 1 shows a typical normalized O−D stretch for the three different ice films used in this study. Following literature precedent and as a result of D_2O molecule coordination differences among these films, this region can be used to distinguish p-ASW, np-ASW, and CI films.[36] In particular, the interface of p-ASW films contains a significant fraction of three- and two-coordinated surface D_2O molecules ("dangling bonds") that can be clearly resolved spectroscopically at 2725 and 2740 cm^{-1}, respectively. Though also present in the np-ASW film, this dangling bond region is much lower intensity, reflecting the large difference in surface areas between porous and non-porous films.[31,37−39] The temperature of the substrate during dosing dictates the water ice morphology; the substrate temperatures used for ice growth were 150 K for CI, 107 K for np-ASW, and 25 K for p-ASW.[7,8]

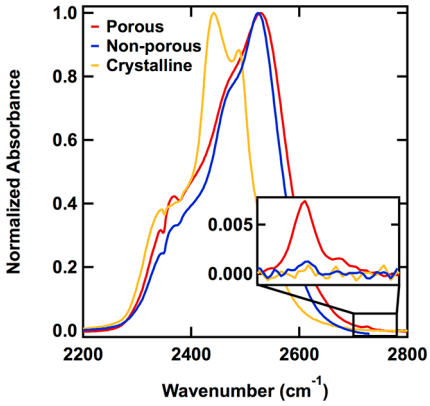

Figure 1. Normalized infrared spectra of the O−D stretch distinguish porous amorphous (p-ASW, green), non-porous amorphous (np-ASW, red), and crystalline (CI, blue) D_2O ices on Au(111) dosed at 25, 107, and 150 K, respectively. The inset demonstrates that while dangling O−D modes are observed for both ASW films they are significantly more intense in the p-ASW films.

ASW films with increased porosity were produced by changing the angle of the directed doser relative to surface normal.[9,40,41] The films used in this study were produced at 30°, 60°, or 70° as well as via background deposition. As characterized by Stevenson et al.,[9] porosity increases with deposition angle, so the D_2O films dosed at 30° are less porous than those grown at 60° or 70°.[42] The pores also grow with an orientation that matches deposition angle.[40] Although films produced via background deposition (backfilling the chamber with water vapor) are as porous as those grown at 70°, the water molecules approach the surface with a thermal energy distribution and random angular orientation resulting in nonuniform pore orientation and size.[40,41] The intensities of the dangling bond spectroscopic signals are known to roughly scale with porosity, so RAIR spectra can be used to qualitatively confirm that ices with different porosities have been formed.[43,44] Unless otherwise specified in this work, "p-ASW" refers to our default porous film grown at 30°, and porous films grown at other deposition angles (60, 70, and background) will be identified as such.

DOI: 10.1021/acs.jpcc.9b03900
J. Phys. Chem. C 2019, 123, 17855−17863

CH_4 beams were produced by expanding 1% CH_4 in H_2 or neat CH_4 at stagnation pressures of 200−400 psi through a 10 μM molybdenum pinhole. Resistively heating the beam nozzle from room temperature to 970 K resulted in CH_4 translational energies of up to 0.3 eV for the neat CH_4 beam and up to 1.8 eV for the CH_4 beam seeded in H_2. The translational energy distribution widths ($\Delta E/E$) ranged from 12% to 21%. Translational energies were measured by time-of-flight (TOF) using a mechanical chopper (a rotating slotted disk) to modulate the beam prior to detection with an in-line quadrupole mass spectrophotometer (QMS). For one experiment (investigating the impact of embedding phenomena), CF_4 beams were produced by expanding 1% CF_4 in H_2 at stagnation pressures of 300−500 psi through a 20 μM molybdenum pinhole. Resistively heating the beam nozzle temperature to over 950 K resulted in a CF_4 translational energy of 5.3 eV with a $\Delta E/E \approx 40\%$.

The CH_4 or CF_4 flux was determined by first measuring the pressure rise with a nude Bayard−Albert ion gauge calibrated to N_2 for a neat CH_4 or CF_4 beam open to the chamber.[25] The flux was then calculated by taking into account the relative gauge sensitivity to CH_4 and N_2,[45,46] or CF_4 and N_2,[45,47] along with the chamber pumping speed, and the spot size of the beam on the Au(111) crystal. Using neat beams at varied stagnation pressures, the calculated fluxes were correlated to a pressure rise for m/z = 15 (CH_4) or for m/z = 69 (CF_4) measured by a RGA not in line with the beam. A linear regression then enabled a conversion between measured RGA pressure and total CH_4 and CF_4 flux. Typical beam fluxes for the CH_4 and CF_4 beams were 2.21×10^{13} atoms cm^{-2} s^{-1} and 1.27×10^{14} atoms cm^{-2} s^{-1}, respectively. All beam exposures in this study were performed at normal incidence.

Sticking probability was determined using the King and Wells technique.[19,48] In order to conduct multiple trials with a given film, the ice was first annealed to 70 K for 30 min. While this reduced porosity slightly, it ensured that repeated King and Wells cycles did not further alter the film morphology throughout the day.[29,40,49] A typical King and Wells experiment conducted at a surface temperature of 33.5 K is shown in Figure 2 where m/z = 15 for CH_4 is monitored as a function of time using an RGA out of line with the beam. The experiment begins with monitoring the background signal prior to introducing any CH_4 into the chamber (P_1). Next, the CH_4 beam is introduced into the chamber, but with a flag in front of the substrate. This pressure rise is the full indirect CH_4 flux (P_2). Then the flag is removed, at which point CH_4 molecules begin sticking to the surface (P_3). The initial sticking probability (S) is thus calculated as

$$S = \frac{(P_2 - P_3)}{(P_2 - P_1)} \quad (1)$$

Over time, the CH_4 signal rises back up to the blocked value as the available surface sites become filled and CH_4 can no longer adsorb onto the surface. The specific challenges with performing King and Wells measurements on the CH_4/ice system are fully addressed in the Discussion section below.

To explore the generalizability of our results, the sticking probabilities for CH_4 on np-ASW, p-ASW, and CI H_2O films were also examined. We note that for all the CH_4 translational energies studied the sticking probability values were the same as those observed for D_2O ices; we did not observe any significant isotopic effect at our experimental resolution, as has been previously detected between D_2O impinging on H_2O and D_2O ices.[50]

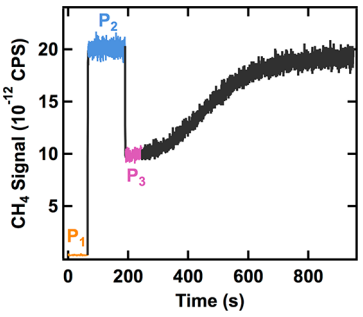

Figure 2. CH_4 signal (m/z = 15) monitored with the RGA during a representative King and Wells experiment conducted at a surface temperature of 33.5 K. P_1 (orange) is the background CH_4 signal; P_2 (blue) is the full CH_4 flux with flag blocking the substrate; P_3 (pink) is CH_4 adsorption with flag removed.

RESULTS

King and Wells. King and Wells measurements of initial sticking probabilities were performed on a prepared ice substrate held at 33.5 K for all results presented in this study. This temperature choice reflects a number of important considerations related to both the nature of the CH_4/D_2O interaction and the King and Wells method itself. As discussed by He et al., there are three potential challenges with performing King and Wells measurements for this ice system.[16] First, the liquid helium cooling of the sample manipulator may impact the pumping speed of the chamber, thereby altering the reflected portion of the beam at different sample temperatures. We avoid this by taking all measurements at a single sample temperature, where the unknown improvement in chamber pumping speed is consistent across experiments. Second, because CH_4 interacts with the ice surface via weak dispersion forces rather than direct chemisorption, these experiments require low surface temperatures. Furthermore, ice surfaces have a wide range of binding sites and binding energies.[39,40,51,52] These two factors present a second challenge; a well-defined saturation of the CH_4-reflected signal might be difficult to observe over short exposure time scales. Although full reflection may ultimately be observed with long exposures, CH_4 desorption as well as finite adsorption of background H_2O and D_2O at these low temperatures over long time scales compete to prevent signal saturation. As such, all initial sticking probability measurements referenced herein are calculated using the initial CH_4 indirect flux rather than the value at saturation. These considerations, therefore, are mitigated by our experimental setup.

Beyond the aforementioned considerations, we are also specifically interested in quantifying the initial sticking probabilities in the low-coverage, submonolayer regime. This is desirable because the concentrations of small molecules in the ISM are typically quite low.[53] Moreover, we want to eliminate any contribution from multilayer sticking, which occurs more readily in porous films, even at higher surface temperatures.[29,42] As such, the desired temperature regime should be high enough to restrict all sticking to the submonolayer.[40] In light of these considerations, 33.5 K was selected as the surface temperature of interest. At this temperature, however, the monolayer is not perfectly stable

DOI: 10.1021/acs.jpcc.9b03900
J. Phys. Chem. C 2019, 123, 17855−17863

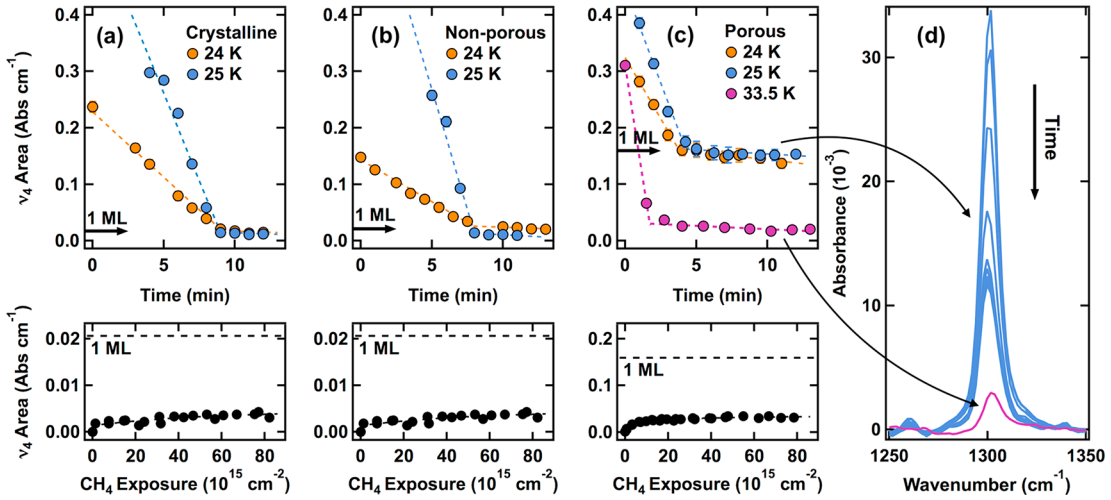

Figure 3. Isothermal desorption of CH_4 from crystalline (CI, a), non-porous amorphous (np-ASW, b), and porous amorphous (185 layers, c) ice films (top) allows for quantitative estimation of monolayer thickness, as measured via the integrated absorbance of the ν_4 mode. Growth of the same peak area during exposure at 33.5 K (bottom) confirms that the amount of adsorbed CH_4 is significantly less than a full monolayer for each type of ice. This is also demonstrated in the corresponding RAIR spectra for desorption a 25 K (blue, d) and 33.5 K (pink, d).

on the surface. While this does not impact the measurements of initial sticking probabilities, CH_4 surface coverage at long exposure time scales will reflect contributions from both adsorption and desorption. By explicitly quantifying and accounting for the rates of desorption, we also account for the third concern with King and Wells measurements, which is that they typically do not have the time resolution to distinguish between molecules that are directly reflected from the surface and those that adsorb for a short time and then desorb again.

As shown in the top panels of Figure 3a–c, quantification of the monolayer was established via isothermal desorption experiments for each ice film. After dosing a multilayer film of CH_4 at 20 K, the integrated area of the ν_4 mode was tracked over time at an elevated temperature.[32,54−56] A distinct slope change is observed when multilayer desorption changes to monolayer, thereby allowing for an approximate quantification of monolayer thickness. The bottom panels of Figure 3a–c show that when the surface is held at 33.5 K (as during a King and Wells experiment) the total amount of adsorbed CH_4 reaches a maximum far below the respective monolayer thickness for each type of ice film. Measured desorption rates for all films at 33.5 K are similar in magnitude to the incident CH_4 flux, so this steady-state maximum indicates that only a small fraction of the monolayer is stable on the surface over long time scales (as shown in Figure 3c in pink).

Figure 3 highlights another important feature of this system, which is that the monolayer thickness (and uptake at 33.5 K) on the porous film is significantly higher than uptake on either CI or np-ASW films (likely due to the increased surface area).[57] This effect has been well-documented previously—Kimmel et al. demonstrated, for example, that a 50 layer film of p-ASW deposited at 30° sees a total CH_4 adsorption of ∼2 monolayer equivalents.[40] On this basis one might expect, therefore, that a 185 layer film (as used in Figure 3c) would likewise adsorb roughly 7−8 monolayers of CH_4. Indeed, the data show that the p-ASW monolayer adsorption is almost exactly 8 times that of the CI and np-ASW films. Similarly, steady-state adsorptions at 33.5 K are on the order of 10^{14} CH_4 cm^{-2} on the porous films and 10^{13} CH_4 cm^{-2} on crystalline and non-porous films.

Sticking Probabilities for CI, np-ASW, and p-ASW. Measured sticking probabilities for CH_4 on crystalline (CI), non-porous (np-ASW), and porous (p-ASW) D_2O films are displayed in Figure 4. Clearly, as the CH_4 incident energy

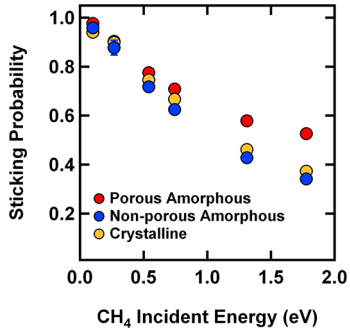

Figure 4. Sticking probabilities for CH_4 on porous (p-ASW, red), non-porous (np-ASW, blue), and crystalline (CI, yellow) D_2O films held at 33.5 K. Sticking probability decreases for all films as incident CH_4 energy increases but remains higher for the porous film. Error bars represent the standard deviation of at least three measurements on at least two different days.

increases, the observed trend on the porous film diverges from both CI and np-ASW; sticking probabilities remain significantly higher for the porous film. This divergence will be discussed in further detail below. First, however, it is important to note that crystalline and non-porous films display nearly identical sticking probability trends throughout the range of incident energies studied. This insensitivity to morphology (CI versus np-ASW) has been observed in other experimental and theoretical systems, including D_2O sticking on H_2O and D_2O,[50] H_2O sticking on H_2O,[17] and CO sticking on H_2O.[6,58] The theoretical work of Al-Halabi et al., for example, shows not only that the sticking of CO is nearly equal between np-ASW and CI H_2O films but also an exponential decay of sticking probability with incident translational energy that is roughly comparable to that measured in this study.[49]

It is important, when discussing adsorption to both porous and non-porous films, to elucidate the contribution of any

DOI: 10.1021/acs.jpcc.9b03900
J. Phys. Chem. C 2019, 123, 17855−17863

penetration of the incident CH_4 into the bulk ice. Previous work in this lab has identified a significant activated uptake channel for incident projectiles in the ice bulk (termed "embedding").[6] After investigating this process for a range of molecules in np-ASW H_2O, a clear momentum barrier for this channel was established (embedding probabilities in CI films were significantly lower than those observed for np-ASW). In general, the momenta reached in the current study (using the relatively light CH_4) are well below this barrier, so no embedding is expected in either np-ASW or CI films. There is, however, the question of whether the use of D_2O (rather than H_2O) or a more porous ice morphology will effectively lower this barrier, making direct comparisons of sticking probabilities across more challenging films. To examine this, both porous and non-porous D_2O ice films were exposed to beams of 5.3 eV CF_4. CF_4 was selected because it has a higher mass and has been successfully used in previous embedding experiments in this lab. All such ballistic embedding experiments were performed with the films held at 70 K to mimic ice preparation conditions used during sticking probability experiments and to preclude a significant surface adsorption channel for CF_4 on the ice. RAIR spectra were collected at regular intervals during exposure to quantify the increase in stable, embedded CF_4 within the ice film (Figure 5a). These growth rates closely

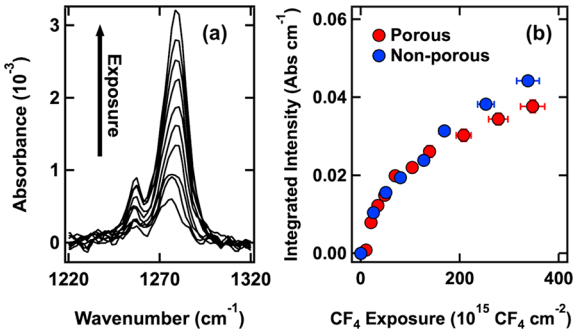

Figure 5. (a) RAIR spectra collected throughout CF_4 exposure show clear signal growth at 1276 and 1257 cm^{-1}. (b) The integrated area of these CF_4 peaks is proportional to the amount of CF_4 that remains embedded in the surface. Both p-ASW and np-ASW films show similar rates of uptake, indicating that the barrier for ballistic embedding into porous films matches that established in previous works for non-porous films. This figure highlights the trend for a porous film deposited at 30° from surface normal, but there are no significant differences in embedding rates for any of the porous films studied in this work.

match data collected in previous works, indicating no major differences between D_2O and H_2O ice films (Figure 5b). Furthermore, the rates of embedding are nearly identical for both p-ASW and np-ASW. Therefore, we expect the previously reported momentum barrier for np-ASW to hold for p-ASW, preventing CH_4 embedding in all of the ice films discussed herein. Indeed, RAIR spectra collected during anneal cycles to 70 K after King and Wells experiments (as well as RGA monitoring of ice desorption at the end of the day) confirm that there is no discernible uptake of CH_4 into the ice bulk; all CH_4 is surface adsorbed.

Though we have demonstrated that there are no differences in embedding phenomena, there are other ways in which CH_4 may interact differently with the p-ASW structure, thereby impacting the observed sticking probability. First, we observe no discernible sputtering of the water film by the CH_4 beam. Though sputtering of astrophysical ices has been reported, the impinging species in these works are typically either charged and/or significantly higher in energy.[24,25] In other words, we do not expect the momentum transfer for the CH_4/D_2O system to be significant enough to desorb water molecules from the surface, nor is there any possibility for electronic sputtering. Second, there is also a large body of research investigating the impact of fast, heavy ions on the morphology of ice films. Specifically, high energy ions (mimicking the effect of cosmic rays) have been shown to compact the pores of vapor-deposited ices.[59−63] Even the relatively low-energy release of H_2 recombination (4.5 eV) on the surface of ice can have a similar compaction effect.[64−67] Though it appears unlikely, it is important to investigate the possible impact that CH_4 may have on the morphology of the porous D_2O films used in this study. Figure 6 depicts representative regions from

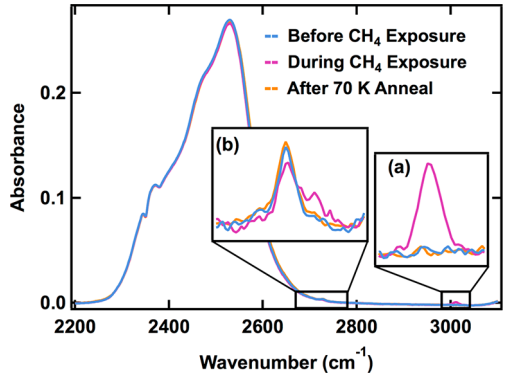

Figure 6. RAIR spectra of D_2O films are unchanged by CH_4 exposure and subsequent anneal. During exposure, some CH_4 adsorbs to the surface (a), and the dangling O−D stretching mode is slightly red-shifted (b). Annealing to 70 K removes all CH_4 and leaves the original D_2O film unchanged.

RAIR spectra of the film before, during, and following CH_4 exposure. Upon exposure to CH_4 (Figure 6a), there is a slight red shift in intensity of the dangling O−D mode (Figure 6b). This shift is well documented in FTIR studies of sequential CH_4/H_2O depositions and indicates that some of the surface D_2O molecules are coordinating with the adsorbed CH_4.[37] After annealing the sample back to 70 K following the experiment, however, all CH_4 desorbs, and there are no lasting changes in the O−D stretch or the dangling O−D peaks. This indicates that the water film height, morphology, and porosity are not impacted by CH_4 sticking experiments, even at the highest energies studied (1.8 eV).

Amorphous Films, Varied Porosity. In the previous section, we established that sticking probabilities of CH_4 are higher for p-ASW films than either np-ASW or CI films at high incident energies. This comparison, however, only includes porous films deposited at 30° relative to surface normal. Figure 7 depicts the sticking probabilities for CH_4 on a variety of porous films, including those deposited via directed doser (at 30°, 60°, and 70° from surface normal) as well as via background deposition. Surprisingly, there is no strong variation in sticking probabilities for CH_4 on any of these films, despite the expected differences in pore orientation and film density.[30,39]

To further understand these results, it is possible to quantify CH_4 coverage on a given surface during a period of exposure

DOI: 10.1021/acs.jpcc.9b03900
J. Phys. Chem. C 2019, 123, 17855−17863

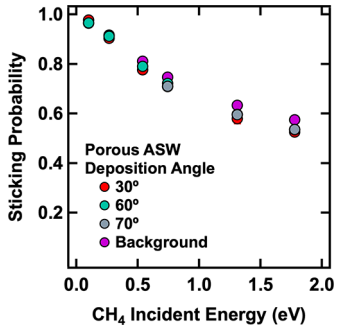

Figure 7. Sticking probabilities are shown for CH_4 impinging on porous D_2O films held at 33.5 K, deposited via directed doser at 30° (red), 60° (green), and 70° (gray) relative to surface normal as well as via background deposition (purple). For the incident energies studied, there are no clear differences in sticking probabilities for these films. Error bars represent the standard deviation of at least three measurements on at least two different days.

and compare it across films. We can estimate the amount of adsorbed CH_4 at a given time t_1 using the following equation

$$N_{CH_4} = (P_2 - P_1)(t_1 - t_0) - \int_{t_0}^{t_1} P(t) \quad (2)$$

In eq 2, P_2 is the indirect CH_4 flux when the beam is blocked from the substrate; P_1 is the background CH_4 pressure when the beam is closed; and t_0 is the time at which the flag is removed; and the film is fully exposed to CH_4. The last term is a simple numerical integration of the raw King and Wells pressure reading between those two time values. In doing this analysis for high translational energy CH_4 beams (1.8 eV), we find that in the first seconds of exposure (corresponding to a total exposure of $(5.0 \pm 0.4) \times 10^{14} \frac{CH_4}{cm^2}$) CI and np-ASW films have adsorbed $(1.0 \pm 0.1) \times 10^{14} \frac{CH_4}{cm^2}$, while 200 ML porous films (at all deposition angles) have accumulated $(1.8 \pm 0.3) \times 10^{14} \frac{CH_4}{cm^2}$. This increase is the result of both increased surface area and higher initial sticking probabilities on porous films at these beam energies, and the difference only widens as exposure continues. The difference in uptake is illustrated qualitatively in Figure 8a, which depicts normalized King and Wells data for representative trials on np-ASW, CI, and p-ASW films. To aid in visual comparison, the data have been normalized in both axes by incident flux. Clearly, the porous film adsorbs more CH_4 before desorption takes over.

In Figure 8b the results of a similar coverage analysis are displayed for all porous ices. In this depiction, total coverage is scaled further by surface area to give an approximate "fractional coverage". Relative surface area is defined via the integrated intensity of the dangling O−D feature. As discussed in Figure 1, this feature provides a reasonable measure of porosity and is related to the total surface area of the film.[41,68] Though the initial sticking probability is consistent across porous films, the relative accumulation of CH_4 is 1−2 times higher for films deposited at 30° and via background deposition than those deposited at 60° or 70°. The roots of this behavior will be addressed further in the Discussion section below.

DISCUSSION

There are two new, significant findings to come out of this work. The first is that the sticking probability of CH_4 on p-

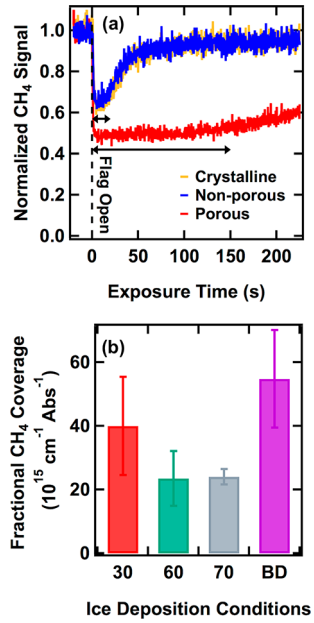

Figure 8. Representative, normalized King and Wells data for all films studied show a clear increase in CH_4 uptake on porous films relative to CI and np-ASW. (a) Total uptake on a porous film (p-ASW, red) is nearly an order of magnitude higher than on either crystalline (CI, yellow) or non-porous (np-ASW, blue). Time and intensity axes are normalized to the incident flux. (b) Fractional CH_4 coverage is higher for porous films deposited at 30° or via background deposition (red, purple) than for those deposited at 60° or 70° (green, gray). Fractional coverage is defined as the total adsorbed CH_4 scaled by the integrated areas of the dangling bond feature. All data were selected from trials using 1.8 eV and CH_4 beams.

ASW D_2O films does not decay as fast as it does on CI and np-ASW D_2O films. The second is that under our energetic conditions the sticking probability trend does not depend on the type of porous ice film used. What follows is a qualitative discussion of why these trends occur and how future studies might further refine the proposed conclusions.

Sticking probabilities for a particular system are known to depend on both the binding energy between the surface and the adsorbate as well as the surface conditions (morphology, temperature, etc.).[44,66] Binding energies for a variety of molecules on different ices of astrochemical interest have been widely reported. As discussed, the low-coverage binding energy for CH_4 on np-ASW ice has been reported in the range of 0.06−0.14 eV.[5] Additionally, differences in binding energy for CO (CH_4 and CO are expected to have similar binding interactions on ice)[39,49,53,69] between CI and np-ASW are small and on the order of 0.01 eV at most.[49] This suggests a partial explanation for the similarity in sticking probabilities between these two ice films. Binding energies on porous films, on the other hand, may be higher than those for either np-ASW or CI ice interfaces. Many studies assert that the binding energy distribution for molecules on porous films is wider and peaks at higher values.[6,70] This idea is refined by Zubkov et al., who concluded that while the distribution of binding sites on the surface is independent of film thickness and porosity the lower fractional coverages of adsorbates on porous films (due to their increased surface area) lead to adsorbates interacting with more higher-energy binding sites.[4,53,71,72] In short, it is likely that at the low coverages investigated here CH_4 binds somewhat more strongly to the porous films.

DOI: 10.1021/acs.jpcc.9b03900
J. Phys. Chem. C 2019, 123, 17855−17863

Binding energy, however, is not a sufficient explanation on its own. Whatever the variation may be for the different ice films, all available reported binding energies for CO and CH_4 are less than 0.2 eV. This is significantly lower than most of the incident energies studied here, suggesting that there must be an additional mechanism for energy accommodation by the surface. Indeed, theoretical work has been done to show that energy dissipation into ice films is incredibly facile under similar conditions.[29] *We suggest, therefore, that it is the distinct morphology of the porous films that is largely responsible for the observed divergence in sticking probabilities at high incident energies.* Desorption studies from a variety of porous substrates have found that desorption kinetics are governed by diffusive motion within pores and multiple collisions with pore walls.[6,73] Indeed, the energy-dissipating effects of these pore wall collisions have been previously cited in studies of molecular or atomic interactions with ice;[74,75] Zubkhov et al. also found that prior to desorption molecules on porous ice experience hundreds of desorption−readsorption attempts (as compared to just one attempt on non-porous).[76] Perhaps the most significant evidence of this energy accommodation by pore walls was demonstrated in a study of HD recombination. Hornekaer et al. found that on porous ice a significant fraction of newly formed HD remained adsorbed to the surface, indicating that the porous network was extremely efficient at dissipating the 4.5 eV recombination energy.[29] This is in contrast to a non-porous film, which saw almost zero retention of the HD molecules following recombination. In summary, the higher sticking probabilities for CH_4 on p-ASW relative to np-ASW and CI likely result from diffusion on and multiple collisions with pore walls, leading to a more efficient dissipation of incident translational energy. It is possible, then, that the sticking probability as discussed here on porous films is more of an uptake coefficient, a measure of advantageous decelleration induced by the physical pore structure, rather than a higher capacity for site-specific energy accommodation on different types of icy surfaces.

In order to discuss CH_4 coverage, it is important to mention the impact of desorption. As mentioned previously, only a fraction of a CH_4 monolayer can remain stably adsorbed on the surface at 33.5 K. Therefore, we expect the increase in reflected signal after the first few seconds (after initial sticking is measured) to be a result of both directly reflected CH_4 and steadily desorbing CH_4. Ultimately, when the reflected signal levels off at long exposure time scales, adsorption and desorption are occurring at equal rates. Measured isothermal, low-coverage desorption rates for all porous films studied here are roughly equivalent and comparable in magnitude to the incident flux, making it possible to compare coverages across these films despite the competing rates of adsorption and desorption.

At normal incidence, this study showed that porous films of any orientation are equally efficient at dissipating the energy of impinging CH_4, but these films adsorb relatively different amounts of CH_4, depending on deposition conditions. The invariance in sticking probability across films of different porosities suggests that the D_2O pore surface is equally efficient at accommodating the incident energy of the CH_4 molecules, regardless of how that pore is oriented relative to the incident beam. These results also suggest, however, that incident CH_4 is not sampling the full surface area of the pore network of 60° and 70° films before beginning to desorb. This can perhaps be understood in terms of pore geometry and size. Films deposited at 30° have lower total surface areas, but they also have pores that are closer to perpendicular to the substrate.[9,77] Relatively more of the pore surface area, therefore, is accessible to the incident beam. Likewise background deposited films have a distribution of pore sizes and orientations, some fraction of which will be perpendicular or near-perpendicular to the substrate. On the other hand, the more tilted, wider pores of the 60° and 70° films present fewer surface sites for the incident beam. *So while CH_4 may undergo multiple collisions with the pore structure before sticking, these coverage results indicate that adsorbed CH_4 is not necessarily diffusing fully into the pore structure and filling up all available surface sites, particularly on the more angled porous film structures.* A future experiment that explores the *angular* dependence of sticking and uptake on these porous films would be a significant step toward identifying the relative importance of factors such as pore orientation and size.

CONCLUSION

In this work we present detailed sticking probability measurements for high translational energy CH_4 impinging on a variety of D_2O ice films at 33.5 K. We confirm that at the energies studied CH_4 is unable to either embed in the bulk or significantly impact the morphology of any ice, including low-density porous films. As incident translational energy increases, the sticking probability decreases for all films. However, CH_4 sticks with greater probability to p-ASW films than it does to either CI or np-ASW films at the same energies. Furthermore, we observe no substantial changes in sticking probability when changing the exact morphology (pore orientation and size) of the porous film used. Even though there may be slight changes in binding energies between CH_4 and the different films, we propose that the porous morphology is largely responsible for this observed divergence. Multiple collisions with pore walls are likely efficient at dissipating the incident energy of the CH_4 projectile. This conclusion is supported by the fact that porous films with more beam-accessible pore surfaces (films deposited at 30° and via background deposition) accumulate relatively more CH_4 during exposure than do films with fewer accessible pore surfaces (deposited at 60° and 70°).

These results are further evidence that the morphology of ice films (and other industrial substrates) critically influences the adsorption and subsequent reactivity of incident molecules. Even if not universally porous, small cracks, fissures, and other morphological deformities in the surface of astrophysical ices may lead to an increased uptake of gaseous molecules, thereby impacting phenomena including the outgassing of comets, chemical reactions in the ISM, and thermal and electrical processing of icy dust grains.[9,68]

AUTHOR INFORMATION

Corresponding Author

*E-mail: s-sibener@uchicago.edu.

ORCID

S. J. Sibener: 0000-0002-5298-5484

Notes

The authors declare no competing financial interest.

ACKNOWLEDGMENTS

This work was supported by the Air Force Office of Scientific Research, Grant Nos. FA9550-15-1-0428 and FA9550-19-1-0324. Support from the NSF-Materials Research Science and

DOI: 10.1021/acs.jpcc.9b03900
J. Phys. Chem. C 2019, 123, 17855−17863

Engineering Center at the University of Chicago, Grant No. NSF-DMR-14-20709, is also gratefully acknowledged.

REFERENCES

(1) Owen, T. The Contributions of Comets to Planets, Atmospheres, and Life: Insights from Cassini-Huygens, Galileo, Giotto, and Inner Planet Missions. *Space Sci. Rev.* **2008**, *138*, 301−316.

(2) Burke, D. J.; Brown, W. A. Ice in Space: Surface Science Investigations of the Thermal Desorption of Model Interstellar Ices on Dust Grain Analogue Surfaces. *Phys. Chem. Chem. Phys.* **2010**, *12*, 5947−5969.

(3) Ayotte, P.; Smith, R. S.; Stevenson, K. P.; Dohnálek, Z.; Kimmel, G. A.; Kay, B. D. Effect of Porosity on the Adsorption, Desorption, Trapping, and Release of Volatile Gases by Amorphous Solid Water. *J. Geophys. Res. Planets* **2001**, *106*, 33387−33392.

(4) Al-Halabi, A.; Van Dishoeck, E. F. Hydrogen Adsorption and Diffusion on Amorphous Solid Water Ice. *Mon. Not. R. Astron. Soc.* **2007**, *382*, 1648−1656.

(5) Hama, T.; Watanabe, N. Surface Processes on Interstellar Amorphous Solid Water: Adsorption, Diffusion, Tunneling Reactions, and Nuclear-Spin Conversion. *Chem. Rev.* **2013**, *113*, 8783−8839.

(6) Al-Halabi, A.; van Dishoeck, E. F.; Kroes, G. J. Sticking of CO to Crystalline and Amorphous Ice Surfaces. *J. Chem. Phys.* **2004**, *120*, 3358−3367.

(7) Jenniskens, P.; Blake, D. F. Crystallization of Amorphous Water Ice in the Solar System. *Astrophys. J.* **1996**, *473*, 1104−1113.

(8) Jenniskens, P.; Blake, D. F.; Kouchi, A. Amorphous Water Ice. In *Solar System Ices, Astrophysics and Space Science Library*; Springer: Dordrecht, 1998; pp 139−155.

(9) Stevenson, K. P.; Kimmel, G. A.; Dohnalek, Z.; Smith, R. S.; Kay, B. D. Controlling the Morphology of Amorphous Solid Water. *Science* **1999**, *283*, 1505−1507.

(10) Angell, C. A. Amorphous Water. *Annu. Rev. Phys. Chem.* **2004**, *55*, 559−583.

(11) Smith, R. S.; Petrik, N. G.; Kimmel, G. A.; Kay, B. D. Thermal and Nonthermal Physiochemical Processes in Nanoscale Films of Amorphous Solid Water. *Acc. Chem. Res.* **2012**, *45*, 33−42.

(12) Bossa, J.-B.; Isokoski, K.; Paardekooper, D. M.; Bonnin, M.; van der Linden, E. P.; Triemstra, T.; Cazaux, S.; Tielens, A. G. G. M.; Linnartz, H. Porosity Measurements of Interstellar Ice Mixtures Using Optical Laser Interference and Extended Effective Medium Approximations. *Astron. Astrophys.* **2014**, *561*, A136.

(13) Isokoski, K.; Bossa, J.-B.; Triemstra, T.; Linnartz, H. Porosity and Thermal Collapse Measurements of H_2O, CH_3OH, CO_2, and H_2O:CO_2 Ices. *Phys. Chem. Chem. Phys.* **2014**, *16*, 3456−3465.

(14) Bartels-Rausch, T.; Bergeron, V.; Cartwright, J. H. E.; Escribano, R.; Finney, J. L.; Grothe, H.; Gutié Rrez, P. J.; Haapala, J.; Kuhs, W. F.; Pettersson, J. B. C.; et al. Ice Structures, Patterns, and Processes: A View across the Icefields. *Rev. Mod. Phys.* **2012**, *84*, 885−944.

(15) Noble, J. A.; Martin, C.; Fraser, H. J.; Roubin, P.; Coussan, S. IR Selective Irradiations of Amorphous Solid Water Dangling Modes: Irradiation vs Annealing Effects. *J. Phys. Chem. C* **2014**, *118*, 20488−20495.

(16) He, J.; Acharyya, K.; Vidali, G. Sticking of Molecules on Nonporous Amorphous Water Ice. *Astrophys. J.* **2016**, *823*, 56.

(17) Batista, E. R.; Ayotte, P.; Bilić, A.; Kay, B. D.; Jónsson, H. What Determines the Sticking Probability of Water Molecules on Ice? *Phys. Rev. Lett.* **2005**, *95*, 223201-1−4.

(18) Watanabe, N.; Kouchi, A. Ice Surface Reactions: A Key to Chemical Evolution in Space. *Prog. Surf. Sci.* **2008**, *83*, 439−489.

(19) King, D. A.; Wells, M. G. Molecular Beam Investigation of Adsorption Kinetics on Bulk Metal Targets: Nitrogen on Tungsten. *Surf. Sci.* **1972**, *29*, 454−482.

(20) Cardillo, M. J.; Balooch, M.; Stickney, R. E. Detailed Balancing and Quasi-Equilibrium in the Adsorption of Hydrogen on Copper. *Surf. Sci.* **1975**, *50*, 263−278.

(21) *The Science of Solar System Ices*; Gudipati, M. S., Castillo-Rogez, J., Eds.; Astrophysics and Space Science Library; Springer New York: New York, NY, 2013; Vol. *356*.

(22) Mousis, O.; Chassefière, E.; Holm, N. G.; Bouquet, A.; Waite, J. H.; Geppert, W. D.; Picaud, S.; Aikawa, Y.; Ali-Dib, M.; Charlou, J.-L.; et al. Methane Clathrates in the Solar System. *Astrobiology* **2015**, *15*, 308−326.

(23) Dartois, E.; Muñoz Caro, G. M.; Deboffle, D.; Montagnac, G.; d'Hendecourt, L. Ultraviolet Photoproduction of ISM Dust. *Astron. Astrophys.* **2005**, *432*, 895−908.

(24) Langlois, G. G.; Li, W.; Gibson, K. D.; Sibener, S. J. Capture of Hyperthermal CO_2 by Amorphous Water Ice via Molecular Embedding. *J. Phys. Chem. A* **2015**, *119*, 12238−12244.

(25) Gibson, K. D.; Langlois, G. G.; Li, W.; Killelea, D. R.; Sibener, S. J. Molecular Interactions with Ice: Molecular Embedding, Adsorption, Detection, and Release. *J. Chem. Phys.* **2014**, *141*, 18C514.

(26) Gibson, K. D.; Killelea, D. R.; Becker, J. S.; Yuan, H.; Sibener, S. J. Energetic Ballistic Deposition of Volatile Gases into Ice. *Chem. Phys. Lett.* **2012**, *531*, 18−21.

(27) Gibson, K. D.; Killelea, D. R.; Yuan, H.; Becker, J. S.; Sibener, S. J. Determination of the Sticking Coefficient and Scattering Dynamics of Water on Ice Using Molecular Beam Techniques. *J. Chem. Phys.* **2011**, *134*, 034703−7.

(28) Huthwelker, T.; Markus Ammann, A.; Peter, T. The Uptake of Acidic Gases on Ice. *Chem. Rev.* **2006**, *106*, 1375−1444.

(29) Zubkov, T.; Smith, R. S.; Engstrom, T. R.; Kay, B. D. Adsorption, Desorption, and Diffusion of Nitrogen in a Model Nanoporous Material. I. Surface Limited Desorption Kinetics in Amorphous Solid Water. *J. Chem. Phys.* **2007**, *127*, 184707.

(30) Herrero, V. J.; Galvez, O.; Mate, B.; Escribano, R. Interaction of CH_4 and H_2O in Ice Mixtures. *Phys. Chem. Chem. Phys.* **2010**, *12*, 3164−3170.

(31) Rowland, B.; Devlin, J. P. Spectra of Dangling OH Groups at Ice Cluster Surfaces and within Pores of Amorphous Ice Infrared Spectra of Ice Surfaces and Assignment of Surface-Localized Modes from Simulated Spectra of Cubic Ice Spectra of Dangling OH Groups at Ice Cluster Surfaces An. *J. Chem. Phys.* **1991**, *94*, 812−813.

(32) Gálvez, Ó.; Maté, B.; Herrero, V. J.; Escribano, R. Spectroscopic Effects in CH_4/H_2 O Ices. *Astrophys. J.* **2009**, *703*, 2101−2107.

(33) Callen, B. W.; Griffiths, K.; Memmert, U.; Harrington, D. A.; Bushby, S. J.; Norton, P. R. The Adsorption of Water on Ni(110): Monolayer, Bilayer and Related Phenomena. *Surf. Sci.* **1990**, *230*, 159−174.

(34) Killelea, D. R.; Gibson, K. D.; Yuan, H.; Becker, J. S.; Sibener, S. J. Dynamics of the Sputtering of Water from Ice Films by Collisions with Energetic Xenon Atoms. *J. Chem. Phys.* **2012**, *136*, 144705.

(35) Engquist, I.; Liedberg, B. D_2O Ice on Controlled Wettability Self-Assembled Alkanethiolate Monolayers: Cluster Formation and Substrate−Adsorbate Interaction. *J. Phys. Chem.* **1996**, *100*, 20089−20096.

(36) Bergren, M. S.; Schuh, D.; Sceats, M. G.; Rice, S. A. The OH Stretching Region Infrared Spectra of Low Density Amorphous Solid Water and Polycrystalline Ice Ih. *J. Chem. Phys.* **1978**, *69*, 3477−3482.

(37) Accolla, M.; Congiu, E.; Dulieu, F.; Manicò, G.; Chaabouni, H.; Matar, E.; Mokrane, H.; Lemaire, J. L.; Pirronello, V. Changes in the Morphology of Interstellar Ice Analogues after Hydrogen Atom Exposure. *Phys. Chem. Chem. Phys.* **2011**, *13*, 8037−8045.

(38) Maté, B.; Rodríguez-Lazcano, Y.; Herrero, V. J. Morphology and Crystallization Kinetics of Compact (HGW) and Porous (ASW) Amorphous Water Ice. *Phys. Chem. Chem. Phys.* **2012**, *14*, 10595.

(39) Raut, U.; Famá, M.; Teolis, B. D.; Baragiola, R. A. Characterization of Porosity in Vapor-Deposited Amorphous Solid Water from Methane Adsorption. *J. Chem. Phys.* **2007**, *127*, 204713.

(40) Kimmel, G. A.; Stevenson, K. P.; Dohnálek, Z.; Smith, R. S.; Kay, B. D.; Smith, R. S.; Kay, B. D. Control of Amorphous Solid Water Morphology Using Molecular Beams. I. Experimental Results. *J. Chem. Phys.* **2001**, *114*, 5284−5294.

DOI: 10.1021/acs.jpcc.9b03900
J. Phys. Chem. C 2019, 123, 17855−17863

(41) Dohnálek, Z.; Kimmel, G. A.; Ayotte, P.; Smith, R. S.; Kay, B. D. The Deposition Angle-Dependent Density of Amorphous Solid Water Films. *J. Chem. Phys.* **2003**, *118*, 364−372.
(42) Smith, R. S.; Zubkov, T.; Dohnalek, Z.; Kay, B. D. The Effect of the Incident Collision Energy on the Porosity of Vapor-Deposited Amorphous Solid Water Films. *J. Phys. Chem. B* **2009**, *113*, 4000−4007.
(43) Buch, V.; Devlin, J. P. Spectra of Dangling OH Bonds in Amorphous Ice: Assignment to 2- and 3-Coordinated Surface Molecules. *J. Chem. Phys.* **1991**, *94*, 4091−4092.
(44) Cholette, F.; Zubkov, T.; Smith, R. S.; Dohnalek, Z.; Kay, B. D.; Ayotte, P. Infrared Spectroscopy and Optical Constants of Porous Amorphous Solid Water. *J. Phys. Chem. B* **2009**, *113*, 4131−4140.
(45) Itikawa, Y. Cross Sections for Electron Collisions with Nitrogen Molecules. *J. Phys. Chem. Ref. Data* **2006**, *35*, 31−53.
(46) Orient, O. J.; Strivastava, S. K. Electron Impact Ionisation of H_2O, CO, CO_2 and CH_4. *J. Phys. B: At. Mol. Phys.* **1987**, *20*, 3923−3936.
(47) Poll, H. U.; Winkler, C.; Margreiter, D.; Grill, V.; Märk, T. D. Discrimination Effects for Ions with High Initial Kinetic Energy in a Nier-Type Ion Source and Partial and Total Electron Ionization Cross-Sections of CF_4. *Int. J. Mass Spectrom. Ion Processes* **1992**, *112*, 1−17.
(48) Matar, E.; Bergeron, H.; Dulieu, F.; Chaabouni, H.; Accolla, M.; Lemaire, J. L. Gas Temperature Dependent Sticking of Hydrogen on Cold Amorphous Water Ice Surfaces of Interstellar Interest. *J. Chem. Phys.* **2010**, *133*, 104507.
(49) Smith, R. S.; May, R. A.; Kay, B. D. Desorption Kinetics of Ar, Kr, Xe, N_2, O_2, CO, Methane, Ethane, and Propane from Graphene and Amorphous Solid Water Surfaces. *J. Phys. Chem. B* **2016**, *120*, 1979−1987.
(50) Morten Hundt, P.; Bisson, R.; Beck, R. D. The Sticking Probability of D_2O-Water on Ice: Isotope Effects and the Influence of Vibrational Excitation. *J. Chem. Phys.* **2012**, *137*, 074701−1−6.
(51) Fayolle, E. C.; Öberg, K. I.; Cuppen, H. M.; Visser, R.; Linnartz, H. Laboratory H_2O:CO_2 Ice Desorption Data: Entrapment Dependencies and Its Parameterization with an Extended Three-Phase Model. *A&A* **2011**, *529*, A74.
(52) Sandford, S. A.; Allamandola, L. J. The Physical and Infrared Spectral Properties of CO_2 in Astrophysical Ice Analogs. *Astrophys. J.* **1990**, *355*, 357−372.
(53) He, J.; Acharyya, K.; Vidali, G. Binding Energy of Molecules on Water Ice: Laboratory Measurements and Modeling. *Astrophys. J.* **2016**, *825*, 89.
(54) Hudson, R. L.; Gerakines, P. A.; Loeffler, M. J. Activation of Weak IR Fundamentals of Two Species of Astrochemical Interest in the T_d Point Group − the Importance of Amorphous Ices. *Phys. Chem. Chem. Phys.* **2015**, *17*, 12545−12552.
(55) Grundy, W. M.; Schmitt, B.; Quirico, E. The Temperature-Dependent Spectrum of Methane Ice I between 0.7 and 5 Mm and Opportunities for Near-Infrared Remote Thermometry. *Icarus* **2002**, *155*, 486−496.
(56) Drobyshev, A.; Aldiyarov, A.; Sokolov, D. IR Spectrometric Studies of Thin Film Cryovacuum Condensates of Methane and Methane-Water Mixtures. *Low Temp. Phys.* **2017**, *43*, 409−415.
(57) Laufer, D.; Kochavi, E.; Bar-Nun, A. Structure and Dynamics of Amorphous Water Ice. *Phys. Rev. B: Condens. Matter Mater. Phys.* **1987**, *36*, 9219−9227.
(58) Kroes, G. J.; Andersson, S. Theory of Molecular Scattering from and Photochemistry at Ice Surfaces. *Proc. Int. Astron. Union* **2005**, *1*, 427−442.
(59) Pratihar, S.; Kohale, S. C.; Yang, L.; Manikandan, P.; Gibson, K. D.; Killelea, D. R.; Yuan, H.; Sibener, S. J.; Hase, W. L. Chemical Dynamics Simulations of High Energy Xenon Atom Collisions with the {0001} Surface of Hexagonal Ice. *J. Phys. Chem. C* **2013**, *117*, 2183−2193.
(60) Johnson, R. E.; Famá, M.; Liu, M.; Baragiola, R. A.; Sittler, E. C.; Smith, H. T. Sputtering of Ice Grains and Icy Satellites in Saturn's Inner Magnetosphere. *Planet. Space Sci.* **2008**, *56*, 1238−1243.
(61) Baragiola, R. A.; Vidal, R. A.; Svendsen, W.; Schou, J.; Shi, M.; Bahr, D. A.; Atteberrry, C. L. Sputtering of Water Ice. *Nucl. Instrum. Methods Phys. Res., Sect. B* **2003**, *209*, 294−303.
(62) Baragiola, R.A.; Atteberry, C.L.; Dukes, C.A.; Fama, M.; Teolis, B.D. Atomic Collisions in Solids: Astronomical Applications. *Nucl. Instruments Methods Phys. Res. Sect. B Beam Interact. with Mater. Atoms* **2002**, *193*, 720−726.
(63) Russo, M. F.; Szakal, C.; Kozole, J.; Winograd, N.; Garrison, B. J. Sputtering Yields for C_{60} and Au_3 Bombardment of Water Ice as a Function of Incident Kinetic Energy. *Anal. Chem.* **2007**, *79*, 4493−4498.
(64) Palumbo, M E; Baratta, G A; Fulvio, D; Garozzo, M; Gomis, O; Leto, G; Spinella, F; Strazzulla, G; et al. Ion Irradiation of Astrophysical Ices. *J. Phys. Conf. Ser.* **2008**, *101*, 012002.
(65) Dartois, E.; Ding, J. J.; de Barros, A. L. F.; Boduch, P.; Brunetto, R.; Chabot, M.; Domaracka, A.; Godard, M.; Lv, X. Y.; Mejía Guamán, C. F.; et al. Swift Heavy Ion Irradiation of Water Ice from MeV to GeV Energies. *Astron. Astrophys.* **2013**, *557*, 1−8.
(66) Mejía, C.; de Barros, A. L. F.; Seperuelo Duarte, E.; da Silveira, E. F.; Dartois, E.; Domaracka, A.; Rothard, H.; Boduch, P. Compaction of Porous Ices Rich in Water by Swift Heavy Ions. *Icarus* **2015**, *250*, 222−229.
(67) Raut, U.; Teolis, B. D.; Loeffler, M. J.; Vidal, R. A.; Famá, M.; Baragiola, R. A. Compaction of Microporous Amorphous Solid Water by Ion Irradiation. *J. Chem. Phys.* **2007**, *126*, 244511.
(68) Kimmel, G. A.; Dohnálek, Z.; Stevenson, K. P.; Smith, R. S.; Kay, B. D. Control of Amorphous Solid Water Morphology Using Molecular Beams. II. Ballistic Deposition Simulations. *J. Chem. Phys.* **2001**, *114*, 5295−5303.
(69) Manca, C.; Martin, C.; Roubin, P. Spectroscopic and Volumetric Characterization of a Non-Microporous Amorphous Ice. *Chem. Phys. Lett.* **2002**, *364*, 220−224.
(70) Noble, J. A.; Congiu, E.; Dulieu, F.; Fraser, H. J. Thermal Desorption Characteristics of CO, O_2 and CO_2 on Non-Porous Water, Crystalline Water and Silicate Surfaces at Submonolayer and Multilayer Coverages. *Mon. Not. R. Astron. Soc.* **2012**, *421*, 768−779.
(71) Fillion, J.-H.; Amiaud, L.; Congiu, E.; Dulieu, F.; Momeni, A.; Lemaire, J.-L. D_2 Desorption Kinetics on Amorphous Solid Water: From Compact to Porous Ice Films. *Phys. Chem. Chem. Phys.* **2009**, *11*, 4396−4402.
(72) Hornekær, L.; Baurichter, A.; Petrunin, V. V.; Luntz, A. C.; Kay, B. D.; Al-Halabi, A. Nfluence of Surface Morphology on D_2 Desorption Kinetics from Amorphous Solid Water. *J. Chem. Phys.* **2005**, *122*, 124701.
(73) Al-Halabi, A.; Kleyn, A. W.; Kroes, G. J. Sticking of HCl to Ice at Hyperthermal Energies: Dependence on Incidence Energy, Incidence Angle, and Surface Temperature. *J. Chem. Phys.* **2001**, *115*, 482−491.
(74) Paldor, A.; Toker, G.; Lilach, Y.; Asscher, M. Xe Interacting with Porous Silicon. *Phys. Chem. Chem. Phys.* **2010**, *12*, 6774−6781.
(75) Villalba, S.; Failache, H.; Lezama, A. Light-Induced Atomic Desorption and Diffusion of Rb from Porous Alumina. *Phys. Rev. A* **2010**, *81*, 032901.
(76) Vidali, G.; Roser, J. E.; Ling, L.; Congiu, E.; Manic, G.; Pirronello, V. The Formation of Interstellar Molecules via Reactions on Dust Grain Surfaces. *Faraday Discuss.* **2006**, *133*, 125−135.
(77) Hornekaer, L.; Baurichter, A.; Petrunin, V. V.; Field, D.; Luntz, A. C. Importance of Surface Morphology in Interstellar H_2 Formation. *Science* **2003**, *302*, 1943−1946.

DOI: 10.1021/acs.jpcc.9b03900
J. Phys. Chem. C 2019, 123, 17855−17863